

Learning a directed acyclic graph with additive heteroscedastic errors

Xintao Xia* Li Chen† Yue Hu‡ Chunlin Li§,¶

Abstract

This paper studies causal discovery for a directed acyclic graph under a structural equation model with additive heteroscedastic errors. We first establish new identifiability results for location-scale noise models, showing that heteroscedasticity can be leveraged to recover causal directions. Based on these insights, we propose a novel iterative procedure, Residual Simultaneous Quantile Estimation (RESQUE), where each iteration consists of a residual-construction stage and a composite quantile regression stage, enabling recursive identification of sink nodes via the invariance of conditional scale coefficients across quantiles. We then establish its theoretical guarantees for recovering topological order and graph structure, even when the number of variables diverges with the sample size. Simulation studies and application to benchmark datasets show that RESQUE performs favorably compared with existing methods, especially when causal information is partly encoded in the variance component. These results highlight exploiting structured variance signals for causal discovery and provide a principled framework for multivariate causal discovery beyond mean-based modeling.

Keywords: Causal discovery; Composite quantile regression; Identifiability; Location-scale noise models.

1 Introduction

Establishing causal relations enables formal reasoning about interventions and counterfactuals, and has been an important topic in modern science and engineering, with applications in biology [43, 31], econometrics [58], psychometrics [6], industrial manufacturing

*Center for Data Science, Zhejiang University. Email: xintaox@zju.edu.cn.

†School of Statistics, University of Minnesota. Email: chen7019@umn.edu.

‡Center for Data Science, Zhejiang University. Email: hy1015@zju.edu.cn.

§Department of Statistics, University of Virginia. Email: chunlin@virginia.edu.

¶Department of Statistics, Iowa State University.

[60], dynamical systems [28], artificial intelligence [44], and other domains. While randomized experiments are the gold standard for causality, they are often unethical or infeasible. Causal discovery aims to learn causal relations among variables from observational data [17], moving beyond statistical associations to determine the direction of effects. It is useful for formulating data-driven conjectures in scientific studies and is viewed as a crucial step towards building automated learning and reasoning systems [44].

Formally, causal relations among variables are often represented using a directed acyclic graph (DAG) [50, 37], a directed graph with no directed cycles, where nodes represent variables of interest, directed edges encode direct causal effects, and the absence of an edge indicates the lack of a direct causal relation. The acyclicity constraint rules out feedback loops, ensuring that the associated data-generating process is well defined [40]. The goal of causal discovery is to reconstruct the underlying DAG.

With solely observational data, determining causal directions is impossible without additional identifiability assumptions on the data-generating process, which is often described by a structural equation model (SEM). Such identifiability assumptions often impose restrictions on the function class or error distributions in the SEM. From a modeling perspective, these conditions reflect a researcher’s inductive bias toward simplicity, modularity, and interpretability in the underlying causal mechanisms. For example, LINGAM assumes linear structural equations while requiring the errors to be non-Gaussian and homoscedastic [47]; SEMs with homoscedastic Gaussian additive errors require the functions to be nonlinear and smooth [40]. Recently, due to the prevalence of heteroscedasticity observed in data, causal models with heteroscedastic errors have received increasing attention [23, 59, 54, 62, 30]; however, they mainly focus on bivariate cases while multivariate causal discovery remains understudied. The challenge is two-fold. First, existing identifiability results [23, 51, 30] are not applicable to bounded variables. It is still unclear under what assumptions the DAG is identifiable when there are bounded and/or unbounded (continuous) variables. Second, likelihood-based methods are prone to parametric misspecification in heteroscedastic models [52, 46], leading to inconsistent estimation. Meanwhile, inde-

pendence testing based methods, such as those based on HSIC [67] or mutual information [51], often require sample splitting and struggle in high dimensions [7], as they do not fully exploit the structured signals in variance components.

In this work, we study causal discovery under an SEM with heteroscedastic errors and address the above questions. Specifically, we contribute to the following aspects:

1. We establish new identifiability results for DAGs with additive heteroscedastic errors. These results unify the identifiability theory for both bounded and unbounded continuous variables in multivariate causal discovery, accommodating practically important yet largely overlooked scenarios. In particular, we find that causal discovery among bounded variables requires much milder conditions than for unbounded variables, thereby complementing the existing theory.
2. We propose a novel iterative estimation procedure, Residual Simultaneous Quantile Estimation (RESQUE), with each iteration consisting of a residual construction step and a composite quantile regression step, integrated with shrinkage techniques to exploit heteroscedastic errors. The proposed approach recursively identifies sink nodes via their parallel conditional quantiles. Thus, it examines error independence rather than optimizing a likelihood function, circumventing the reliance on parametric specification. It exploits the structured, sparse signals in variance components by transforming independence testing to feature selection. In this way, RESQUE avoids sample splitting and many high-dimensional (nonparametric) independence tests, leading to improved performance in causal discovery.
3. We analyze the theoretical properties of RESQUE and prove its consistency for order and graph estimation. The simulations and real-data benchmarks demonstrate the strong performance of RESQUE, consistent with our motivation and theoretical analysis.

The central message is two-fold: bounded variables help with the identifiability of heteroscedastic SEMs, and structured causal signals in heteroscedastic patterns should be

exploited for multivariate causal discovery.

Related work. Causal discovery has been extensively studied; see [21, 17, 56] for comprehensive reviews. Broadly, there are four distinct but interconnected approaches to causal discovery from solely observational data. (a) Constraint-based methods [49, 19, 48] test conditional independence to infer the underlying causal graph up to its Markov equivalence classes. (b) Asymmetry-based methods exploit the algebraic asymmetry implied by SEMs to determine the causal order. Prominent examples include order-based approaches [40, 69] and independent component analysis approaches [47, 65]. (c) Score-based methods estimate the causal graph by optimizing a certain criterion function over a discrete [12] or a continuous search space [70, 26]. (d) Hybrid methods [55, 10] seek to combine a constraint-based approach with an asymmetry- or score-based approach. Our work belongs to the family of asymmetry-based methods.

Among the above approaches, (b)–(d) often introduce an SEM, also called functional causal model, to describe the data-generating process, where the underlying DAG is induced by the SEM. Thus, the identifiability of the SEM has been a central topic in causal discovery [47, 66, 65, 22, 39, 40, 9, 36]. Notably, [47] studies multivariate linear SEMs with non-Gaussian errors; [65] comprehensively characterizes bivariate post-nonlinear causal models; [40] thoroughly discusses the identifiability of multivariate additive noise models (ANMs); and [23, 51, 30] offer identifiability results for heteroscedastic SEMs. Nonetheless, most work has focused exclusively on continuous variables with full (unbounded) support. Exceptions include [39], which discusses ANMs with discrete variables, and [9], which studies ANMs with compactly supported variables and smooth monotonic functional relations. Our work adds to the prior literature by offering a unifying identification for multivariate heteroscedastic SEMs with bounded and unbounded continuous variables.

Organization. The rest of the paper is organized as follows. Section 2 introduces the additive heteroscedastic causal model and presents the identifiability results. Section 3 describes the proposed finite-sample estimation method and Section 4 establishes its the-

oretical properties. Section 5 examines the method through simulation studies and real data benchmarks. Finally, Section 6 concludes the paper with a discussion of extensions and future directions.

2 Heteroscedastic causal model and identifiability

We first introduce the basic terminology of DAGs. A DAG is defined as a graph in which every edge is directed, and the graph does not contain any loops or cycles. Let $G = (V, E)$ be a DAG associated with a random vector $\mathbf{X} \in \mathbb{R}^p$. The node set of $V = \{X_1, \dots, X_p\}$ indexes the components of \mathbf{X} , and a directed edge $(i, j) \in E$ encodes a direct causal relationship from X_i to X_j . If $(i, j) \in E$, then X_i is called a parent of X_j , and X_j is called a child of X_i . The set of parents of X_j is denoted by $\text{PA}^G(j)$, and the set of children of X_i is denoted by $\text{CH}^G(i)$. If there exists a directed path from X_j to X_k in G , then X_j is called an ancestor of X_k . The set of all ancestors of X_j , including X_j , is denoted by $\text{AN}^G(j)$, while the set of strict ancestors is denoted by $\text{an}^G(j) = \text{AN}^G(j) \setminus \{j\}$. The set of all non-descendants of X_j , including X_j , is denoted by $\text{ND}^G(j)$.

We consider the following data-generating procedure: *independent and identically distributed* (i.i.d.) realizations of the random vector $\{X_j\}_{j=1}^p$ are generated according to a *structural equation model* (SEM) associated with a DAG [37]:

$$X_j = h_j(\mathbf{X}_{\text{PA}^G(j)}, \varepsilon_j) \quad \text{for } j = 1, \dots, p,$$

where $\{\varepsilon_1, \dots, \varepsilon_p\}$ are mutually independent random errors, and $h_j(\cdot) : \mathbb{R}^{|\text{PA}^G(j)|+1} \rightarrow \mathbb{R}$ are unknown functions. Lacking additional assumptions on the SEM, the underlying DAG G is identifiable only up to its Markov equivalence class. Given a DAG $G = (V, E)$, a permutation π , defined as a bijection from the node set $[p]$ to $[p]$, is considered a *topological order* (*causal order*) of G if, for any $X_i, X_j \in V$, such that X_i is an ancestor of X_j , we have $\pi(i) < \pi(j)$. See Definition 1 for a formal statement. A permutation π , represented by its ordered sequence $(\pi(1), \dots, \pi(p))$, does not in general uniquely determine a DAG. For example, the causal order $(1, 2, 3)$ is compatible with multiple DAGs, including one with

directed edges $X_1 \rightarrow X_2 \rightarrow X_3$ and another with only a single edge $X_1 \rightarrow X_2$. Conversely, a DAG may admit multiple causal orders. Nevertheless, a topological order remains highly informative. We study its identifiability as a first step toward identifying the DAG.

Definition 1. We say that the algorithm recovers a topological order π over the DAG if

$$\pi(i) < \pi(j) \quad \text{implies} \quad j \notin \text{an}(i, G) \quad \text{for all} \quad i, j \in V.$$

To fully exploit the information contained in the error distribution, we consider a general *location-scale noise model* (LSNM) allowing the noise to depend on parent variables:

$$X_j = f_j(\mathbf{X}_{\text{PA}^G(j)}) + g_j(\mathbf{X}_{\text{PA}^G(j)})\varepsilon_j, \quad (1)$$

where $f_j(\cdot) : \mathbb{R}^{|\text{PA}^G(j)|} \rightarrow \mathbb{R}$ and $g_j(\cdot) : \mathbb{R}^{|\text{PA}^G(j)|} \rightarrow \mathbb{R}^+$ are unknown functions. We first study the bivariate case and then extend the analysis to the general multivariate setting.

Assumption 1 (Bivariate Identifiability). Suppose the two-variable SEM (1) given by: $X_i = \varepsilon_i$ and $X_j = f(X_i) + g(X_i)\varepsilon_j$, where f, g are not constant functions and the joint distribution of (X_i, X_j) is absolutely continuous. For any reverse SEM, $X_i = h(X_j) + k(X_j)\tilde{\varepsilon}_i$ and $X_j = \tilde{\varepsilon}_j$, with densities $p_{X_j}(\cdot)$ and $p_{\tilde{\varepsilon}_i|X_j}(\cdot|\cdot)$, one of the following conditions must hold:

1. Let $\nu_1(\cdot) := \log p_{X_j}(\cdot)$, $\nu_2(\cdot, \cdot) := \log p_{\tilde{\varepsilon}_i|X_j}(\cdot|\cdot)$, and f, g, h, k be twice-differentiable.

The following equation fails to hold for all x_i, x_j satisfying $p_{X_j}(x_j) > 0$, $p_{\tilde{\varepsilon}_i|X_j}(x_i|x_j) > 0$ and $H(x_i, x_j) \neq 0$, where $H(x_i, x_j) = g(x_i)f'(x_i) + g'(x_i)[x_j - f(x_i)]$:

$$0 = \nu_1''(x_j) + \frac{g'(x_i)}{H(x_i, x_j)}\nu_1'(x_j) + \left(\frac{\partial^2}{\partial x_j^2} + \frac{g(x_i)}{H(x_i, x_j)} \frac{\partial^2}{\partial x_j \partial x_i} + \frac{g'(x_i)}{H(x_i, x_j)} \frac{\partial}{\partial x_j} \right) \nu_2(x_i, x_j).$$

2. Let $\nu_3(\cdot, \cdot) := p_{X_i|X_j}(\cdot|\cdot)$, and f, g, h, k be differentiable. The error distributions in (1) have continuous support, and X_i has bounded support. Define $s(x) := \text{ess sup}(X_i | X_j = x) - \text{ess inf}(X_i | X_j = x)$ and $\ell(x) := \text{ess inf}(X_i/s(x) | X_j = x)$, where $\text{ess sup}(X_i|X_j)$ (respectively, $\text{ess inf}(X_i|X_j)$) denotes the smallest upper (largest lower) bound of the conditional distribution that holds almost surely. Either the set $\{x_i \in$

$\mathbb{R} : p_{X_i|X_j}(x_i | x_j) > 0\}$ is disconnected for some x_j with $p_{X_j}(x_j) > 0$, or the following equation fail to hold for $z = x_i/s(x) - \ell(x)$ whenever $p_{X_j}(x_j) > 0$, $p_{X_i|X_j}(x_i|x_j) > 0$:

$$0 = s'(x)\nu_3(z, x) + s(x) \left[\partial_z \nu_3(z, x) \{s'(x)(z + \ell(x)) + s(x)\ell'(x)\} + \partial_x \nu_3(z, x) \right].$$

Theorem 1. *Suppose the joint distribution of (X_1, X_2) satisfies Assumption 1 with underlying graph G . Then G is identifiable from the joint distribution of (X_1, X_2) .*

Theorem 1 establishes identifiability in the bivariate setting without requiring unbounded support, thereby relaxing a key assumption commonly imposed in the literature. The first condition is adopted from [23], while the second leverages bounded domains to obtain identifiability in a broader class of models. In addition, due to space constraints, we establish identifiability via the boundary property in the Appendix.

Theorem 2 (Identification of DAG). *Let $\mathbf{X} \in \mathbb{R}^p$ be generated according to the location–scale noise structural equation model in (1) with underlying DAG G and the joint distribution of \mathbf{X} is absolutely continuous. Assume that for every $j \in [p]$, every $i \in PA^G(j)$, and every set $\mathcal{S} \subseteq [p]$ with $PA^G(j) \setminus \{i\} \subseteq \mathcal{S} \subseteq ND^G(j) \setminus \{i, j\}$. Define $\mathcal{S}_1 = PA^G(j) \setminus \{i\}$ and $\mathcal{S}_2 = \mathcal{S} \setminus \mathcal{S}_1$. There exists a realization $\mathbf{x}_{\mathcal{S}}$ satisfying $p_{\mathbf{X}_{\mathcal{S}}}(\mathbf{x}_{\mathcal{S}}) > 0$, where $p_{\mathbf{X}_{\mathcal{S}}}(\cdot)$ denotes the marginal density of $\mathbf{X}_{\mathcal{S}}$, and the following conditions hold. Define the pseudo-variables $X_j^* := f_j(X_i^*, \mathbf{x}_{\mathcal{S}_1}) + g_j(X_i^*, \mathbf{x}_{\mathcal{S}_1})\varepsilon_j$ and $X_i^* \sim \mathcal{L}(X_i | \mathbf{X}_{\mathcal{S}} = \mathbf{x}_{\mathcal{S}})$. Then the pair (X_i^*, X_j^*) satisfies Assumption 1. Then G is identifiable from the joint distribution of \mathbf{X} .*

Theorem 2 establishes identifiability of the DAG under a multivariate location–scale noise model. For each parent–child pair, it requires the existence of a conditioning under which the resulting conditional random variables (pseudo-variables) satisfy the bivariate identifiability assumptions. These conditions are local, requiring only a single realization with positive density. The result mirrors and extends the additive noise model identifiability results of [38], providing a principled foundation for causal discovery in multivariate nonlinear models with heteroskedastic noise.

3 Residual simultaneous quantile estimation

In this section, we develop a causal discovery procedure based on conditional quantile functions. We first identify the topological order and then recover the causal graph.

3.1 Recovering topological order

In this section, we introduce a method that leverages comparisons of conditional quantile functions to iteratively identify sink nodes and thereby recover a topological ordering of the variables. Suppose that we observe n *independent and identically distributed* (i.i.d.) samples $\{\mathbf{X}_i = (X_{i,1}, \dots, X_{i,p})^\top\}_{i=1}^n$ generated according to the model in (1),

$$X_{i,j} = f_j(\mathbf{X}_{i,\text{PA}^G(j)}) + g_j(\mathbf{X}_{i,\text{PA}^G(j)})\varepsilon_{i,j} \quad \text{for } i = 1, \dots, n; j = 1, \dots, p.$$

For each $j = 1, \dots, p$, we approximate $f_j(\mathbf{X}_{\text{PA}^G(j)})$ and $\log g_j(\mathbf{X}_{\text{PA}^G(j)})$ via linear combinations of the feature maps $\Phi(\mathbf{X}_{\text{PA}^G(j)})$ and $\Psi(\mathbf{X}_{\text{PA}^G(j)})$, respectively. Here, $\Phi(\cdot)$ and $\Psi(\cdot)$ represent feature transformations, such as polynomial basis expansions of $\mathbf{X}_{\text{PA}^G(j)}$. To simplify notation, for any index set $A \subset [p]$ and integer $c_d \in \mathbb{N}$, we write $\Phi(\mathbf{X}_A)$ and $\Psi(\mathbf{X}_A)$ for feature maps that send $\mathbf{X}_A \in \mathbb{R}^{|A|}$ to $\mathbb{R}^{c_d \times |A|}$. We assume that these feature maps are monotone in the sense that, for any $A \subset B \subset [p]$, $\text{span}(\Phi(\mathbf{X}_A)) \subset \text{span}(\Phi(\mathbf{X}_B))$ and $\text{span}(\Psi(\mathbf{X}_A)) \subset \text{span}(\Psi(\mathbf{X}_B))$ for $A \subset B \subset [p]$. It remains to consider the model:

$$X_j = \Phi(\mathbf{X}_{\text{PA}^G(j)})^\top \beta_j^* + r_j^{(f)} + \exp\{\Psi(\mathbf{X}_{\text{PA}^G(j)})^\top \gamma_j^* + r_j^{(g)}\} \varepsilon_j, \quad (2)$$

where β_j^* and γ_j^* are best-approximation parameters, to be defined below, and $r_j^{(f)}, r_j^{(g)}$ represent the approximation errors for $f_j(\mathbf{X}_{\text{PA}^G(j)})$ and $\log g_j(\mathbf{X}_{\text{PA}^G(j)})$, respectively.

As a first step, we obtain the residuals by fitting a least squares regression model. We consider p regression problems of the form regressing X_j on $\Phi(\mathbf{X}_{-j})$ for $j = 1, \dots, p$. For each j , we define the empirical loss function $\mathcal{L}_{n,j}(\cdot) : \mathbb{R}^{c_d(p-1)} \rightarrow \mathbb{R}$ by

$$\mathcal{L}_{n,j}(\beta) = \frac{1}{n} \sum_{i=1}^n \{X_{i,j} - \Phi(\mathbf{X}_{i,-j})^\top \beta\}^2 / 2 + \lambda_1 \|\beta\|_1 \quad (3)$$

where $\lambda_1 > 0$ is a tuning parameter, and $\mathbf{X}_{i,-j}$ denotes \mathbf{X}_i with its j th component removed. The corresponding population parameter β_j^* in (2) is defined as $\beta_j^* = \arg \min_{\beta} \mathbb{E}[(X_j -$

$\Phi(\mathbf{X}_{-j})^\top \beta)^2]$. Let $\widehat{\beta}_j = \arg \min_{\beta} \mathcal{L}_{n,j}(\beta)$ denote the corresponding sample estimator. We then define the estimated residuals as $\widehat{Y}_{i,j} := \log |X_{i,j} - \Phi(\mathbf{X}_{i,-j})^\top \widehat{\beta}_j|$ for all i, j .

Let $0 < \tau_1 < \dots < \tau_K < 1$ be K quantiles of interest. We next estimate the conditional quantile functions $Q_{\tau_k}(\widehat{Y}_j | \mathbf{X}_{-j})$ for $k \in \{1, \dots, K\}$. Since its introduction by [25], quantile regression has become a standard approach for estimating conditional quantile functions. Note that the conditional τ th quantile function satisfies the following population estimating equation:

$$(\gamma_{j,k}, b_{j,k}) = \underset{\gamma, b}{\operatorname{argmin}} \mathbb{E}[\rho_{\tau_k}(Y_j - \Psi(\mathbf{X}_{-j})^\top \gamma - b)],$$

where $Y_j := \log |X_j - r_j^{(f)} - \Phi(\mathbf{X}_{-j})^\top \beta^*|$ and $\rho_\tau(u) = u\{\tau - 1(u \leq 0)\}$ is the check function. When X_j is a sink node, the coefficient $\gamma_{j,k}$ is invariant across quantile levels and coincides with γ_j^* on the components associated with $\Psi(\mathbf{X}_{\text{PA}^G(j)})$, while all remaining components are zero. We next consider a penalized composite quantile regression model to identify the sink nodes. For simplicity, we assume that the distribution of ε_j is continuous, so that the quantile-specific intercepts $b_{j,k}$ are uniquely defined. Given the estimated residuals $\widehat{Y}_{i,j}$, we formulate the following penalized quantile regression problem:

$$\begin{aligned} & \{(\widehat{\gamma}_{j,k}, \widehat{b}_{j,k})\}_{k=1}^K \\ &= \underset{(\gamma_k, b_k)_{k=1}^K}{\operatorname{argmin}} \sum_{k=1}^K \left\{ \frac{1}{n} \sum_{i=1}^n \rho_{\tau_k}(\widehat{Y}_{i,j} - \Psi(\mathbf{X}_{i,-j})^\top \gamma_k - b_k) + \lambda_2 \|\gamma_k\|_1 \right\} + \sum_{k=1}^K P_{\lambda_3}(\|\gamma_k - \gamma_{k+1}\|_2), \end{aligned}$$

where $P_{\lambda_3}(\cdot)$ is a penalty function to be specified later, λ_2 and λ_3 are tuning parameters, and we adopt the convention $\gamma_{K+1} = \gamma_1$. A node is identified as a sink node if all estimated coefficient vectors $\widehat{\gamma}_k$ for $1 \leq k \leq K$ are shrunk to the same value. We then remove all identified sink nodes from $[p]$ and apply the proposed procedure to the remaining nodes. This process is repeated until all nodes are identified. This iterative identification of sink nodes induces a topological ordering of the variables in reverse: nodes identified earlier appear later in the order. By successively removing sink nodes, we recover the topological order from sinks to sources (see Figure 1).

We next address the computational aspects of the proposed procedure. The penalized optimization problem in the first-stage mean regression can be solved efficiently via

proximal gradient descent. For the second-stage penalized quantile regression, we adopt a general folded concave penalty [14], which satisfies the following properties:

1. $P_\lambda(t)$ is increasing and concave in $t \in [0, \infty)$ with $P_\lambda(0) = 0$;
2. $P_\lambda(t)$ is differentiable in $t \in [0, \infty)$ with $P'_\lambda(+0) \geq a_1\lambda$;
3. $P'_\lambda(t) \geq a_1\lambda$ for $t \in (0, a_2\lambda]$;
4. $P'_\lambda(t) = 0$ for $t \in [a\lambda, \infty)$ with pre-specified constant $a > a_2$.

The above class of penalties includes SCAD [13] and MCP [64] as special cases. The resulting optimization problem can be efficiently solved via the local linear approximation (LLA) algorithm. Let $\{(\hat{\gamma}_{j,k}^{(0)}, \hat{b}_{j,k}^{(0)})\}_{k=1}^K$ denote the solution to the penalized composite quantile regression problem

$$(\hat{\gamma}_{j,k}^{(0)}, \hat{b}_{j,k}^{(0)})_{k=1}^K = \operatorname{argmin}_{(\gamma_k, b_k)_{k=1}^K} \sum_{k=1}^K \left\{ \frac{1}{n} \sum_{i=1}^n \rho_{\tau_k}(\hat{Y}_{i,j} - \Psi(\mathbf{X}_{i,-j})^\top \gamma_k - b_k) + \lambda_2 \|\gamma_k\|_1 \right\},$$

which yields a convex optimization problem that can be solved efficiently using linear programming [29]. The corresponding LLA-based optimizer is given by

$$\begin{aligned} (\hat{\gamma}_{j,k}, \hat{b}_{j,k})_{k=1}^K = \operatorname{argmin}_{(\gamma_k, b_k)_{k=1}^K} & \sum_{k=1}^K \left\{ \frac{1}{n} \sum_{i=1}^n \rho_{\tau_k}(\hat{Y}_{i,j} - \Psi(\mathbf{X}_{i,-j})^\top \gamma_k - b_k) + \lambda_2 \|\gamma_{j,k}\|_1 \right\} \\ & + \sum_{k=1}^K P'_{\lambda_3}(\|\hat{\gamma}_{j,k}^{(0)} - \hat{\gamma}_{j,k+1}^{(0)}\|_2) \|\gamma_{j,k} - \gamma_{j,k+1}\|_2, \end{aligned} \quad (4)$$

where $P'_{\lambda_3}(\cdot)$ denotes the derivative of $P_{\lambda_3}(\cdot)$. In practice, for a given λ_3 , the estimated parameters $\hat{\gamma}_{j,k}$ for $j = 1, \dots, p$ may not be exactly shrunk to the same value due to finite-sample variability. In such cases, we propose selecting the node that minimizes the discrepancy measure $\sum_{k=1}^K \|\hat{\gamma}_k - \hat{\gamma}_{k+1}\|_2$ as the sink node, and then proceeding with the iterative identification procedure.

3.2 Recovering graph structure

The proposed method can be further extended to recover the underlying graph structure. When X_j is identified as a sink node, under the additive location–scale model (1),

$X_j = f_j(\mathbf{X}_{\text{PA}^G(j)}) + g_j(\mathbf{X}_{\text{PA}^G(j)})\varepsilon_j$, there exists a directed edge from node l to node j if and only if either $f_j(\mathbf{X}_{\text{PA}^G(j)})$ or $g_j(\mathbf{X}_{\text{PA}^G(j)})$ is nonconstant as X_l varies. With basis expansions, consider the working model $X_j = \Phi(\mathbf{X}_{-j})^\top \beta_j + \exp\{\Psi(\mathbf{X}_{-j})^\top \gamma_j^*\} \varepsilon_j$. Under this representation, the above condition can be reformulated as a *variable-selection* problem. Specifically, there is a directed edge from node l to node j if and only if there exists an index $q > 0$ such that either (i) $[\beta_j]_q \neq 0$ and $[\Phi(\mathbf{X}_{-j})]_q$ is not a constant function of X_l , or (ii) $[\gamma_{j,1}]_q \neq 0$ and $[\Psi(\mathbf{X}_{-j})]_q$ is not a constant function of X_l , where $[\cdot]_q$ denotes the q th component of a vector.

Building on the estimation procedures in (3) and (4), we develop two approaches for graph recovery. We first adopt general folded concave penalties together with the local linear approximation (LLA) algorithm to achieve selection consistency. Given the preliminary estimates $\hat{\beta}_j$ and $\hat{\gamma}_{j,1}$, we define the following one-step LLA estimators:

$$\begin{aligned} \hat{\beta}_j^c &= \arg \min_{\beta} \frac{1}{n} \sum_{i=1}^n \{X_{i,j} - \Phi(\mathbf{X}_{i,-j})^\top \beta\}^2 / 2 + \sum_l P'_{\lambda_1^c}(|\hat{\beta}_{j,l}|) |\beta_l|, \\ \hat{\gamma}_{j,1}^c &= \arg \min_{\gamma, b} \frac{1}{n} \sum_{i=1}^n \rho_{\tau_1}(\hat{Y}_{i,j} - \Psi(\mathbf{X}_{i,-j})^\top \gamma - b) + \sum_l P'_{\lambda_2^c}(|\hat{\gamma}_{j,1,l}|) |\gamma_l|, \end{aligned} \tag{5}$$

where λ_1^c, λ_2^c are penalties, and the summation over l ranges over all components. Since all $\hat{\gamma}_{j,k}$ are shrunk to the same value, we use $\hat{\gamma}_{j,1}$ for illustration. As established by [14], under suitable regularity conditions the estimators $\hat{\beta}_j^c, \hat{\gamma}_{j,1}^c$ are *sign-consistent* [68], which in turn implies selection consistency. We also consider a second, computationally simpler approach based on hard thresholding. Specifically, the basis functions $[\Phi(\mathbf{X}_{-j})]_q$ and $[\Psi(\mathbf{X}_{-j})]_q$ are selected whenever $|[\Phi(\mathbf{X}_{-j})]_q| \geq a_n$ and $[\Psi(\mathbf{X}_{-j})]_q \geq b_n$, respectively, for two sequences of positive thresholds. As will be shown in Section 4, this hard-thresholding procedure consistently recovers the graph G under slightly stronger assumptions than those required for general folded concave penalties, while offering substantial computational advantages. The complete algorithm is summarized in Algorithm 1.

Algorithm 1 Regression with subsequent quantile check (RESQUE)

Require: Data $\{\mathbf{X}_i\}_{i=1}^n$, quantile $\{\tau_k\}_{k=1}^K$;

Ensure: Estimated topological order π and underlying graph \widehat{G} ;

1: Initialize $S = [p]$, $\pi = [\cdot]$, $\widehat{G} = \emptyset$;

2: **repeat**

3: Regress X_j on $\{X_l\}_{l \in S \setminus \{j\}}$ by (3) and regress the residual on $\{X_l\}_{l \in S \setminus \{j\}}$ by (4) to obtain $\widehat{\beta}_j^S, \widehat{\gamma}_{j,1}^S, \dots, \widehat{\gamma}_{j,K}^S$ for all $j \in S$;

4: **for** $j \in S$ **do**

5: **if** $\widehat{\gamma}_{j,1}^S = \dots = \widehat{\gamma}_{j,K}^S$ **then**

6: Update topological order by $\pi := [j, \pi]$ and update $S := S \setminus \pi$;

7: Concave penalty method: run the regressions models (5) with initial estimates $\widehat{\beta}_j^S, \widehat{\gamma}_{j,1}^S$; update the estimated graph \widehat{G} through

$$\begin{aligned} \widehat{\text{pa}}(j) := & \{i \in S : \exists q \text{ s.t. } [\widehat{\beta}_j^C]_q \neq 0 \text{ and } [\Phi(\{X_l\}_{l \in S \setminus \{j\}})]_q \text{ contains } X_i\} \\ & \cup \{i \in S : \exists q \text{ s.t. } [\widehat{\gamma}_{j,1}^C]_q \neq 0 \text{ and } [\Psi(\{X_l\}_{l \in S \setminus \{j\}})]_q \text{ contains } X_i\}; \end{aligned}$$

8: Hard-thresholding method: let t be a positive number depending on the current topological order π , and update the estimated graph \widehat{G} by the following criterion,

$$\begin{aligned} \widehat{\text{pa}}(j) := & \{i \in S : \exists q \text{ s.t. } |[\widehat{\beta}_j^S]_q| \geq t \text{ and } [\Phi(\{X_l\}_{l \in S \setminus \{j\}})]_q \text{ contains } X_i\} \\ & \cup \{i \in S : \exists q \text{ s.t. } |[\widehat{\gamma}_{j,1}^S]_q| \geq t \text{ and } [\Psi(\{X_l\}_{l \in S \setminus \{j\}})]_q \text{ contains } X_i\}; \end{aligned}$$

9: **end if**

10: **end for**

11: **until** $S = \emptyset$;

4 Theory

This section studies the theoretical properties of RESQUE. The results are organized into two parts. First, we present convergence guarantees for the proposed regression estimators. Then, we establish consistency results for the estimated topological ordering and graph obtained by RESQUE.

4.1 Convergence rates for regressions

We present the theoretical properties of the proposed regression procedures. For each $j = 1, \dots, p$, under model (2), define the true parameter β_j as

$$\beta_j = \arg \min_{\beta} \mathbb{E}[(X_j - \Phi(\mathbf{X}_{-j})^\top \beta)]^2. \quad (6)$$

The corresponding approximation error is given by $r_j^{(f)} = \mathbb{E}(X_j | \mathbf{X}_{-j}) - \Phi(\mathbf{X}_{-j})^\top \beta_j$. The regression error is define as $\varepsilon'_j = X_j - \mathbb{E}(X_j | \mathbf{X}_{-j})$. We impose the following conditions on the covariate $\Phi(\mathbf{X}_{-j})$ for $j = 1, \dots, p$ and regression error ε'_j .

Assumption 2. Model (2) satisfies $\|\beta_j\|_0 \leq s_1$ and $\|r_j^{(f)}\|_2^2 \leq C s_1/n$ for a constant $C > 0$ and $j \in [p]$. The variance of ε'_j are bounded from above by a constant C and the k th component of $\Phi(\mathbf{X}_{-j})\varepsilon'_j$ satisfies Cramér's condition for $1 \leq j \leq p$, $1 \leq k \leq c_d \cdot p$.

Assumption 2 assumes the regression coefficients in (6) are sparse, and the approximation errors are relatively small. Such conditions are standard in high-dimensional literature [4, 5, 24]. For the variance condition, when X_j is a sink node, the regression error ε'_j coincides with $\exp\{\Psi(\mathbf{X}_{\text{PA}^G(j)})^\top \gamma_j^* + r_j^{(g)}\} \varepsilon_j$. In this case, the finite variance condition is equivalent to requiring that $\exp\{\Psi(\mathbf{X}_{i,\text{PA}^G(j)})^\top \gamma_j^* + r_{i,j}^{(g)}\}$ be bounded and that ε_j have finite variance. When X_j is not a sink node, the regression error has a smaller variance than the structural error due to conditioning.

Assumption 3. For $\forall j \in [p]$ and some constant $c_0 \geq 1$, define $A_j = \{\beta \mid \|\beta_{T_j^c}\|_1 \leq c_0 \|\beta_{T_j}\|_1\}$, where T_j is the support of β_j . The sample covariance matrix satisfies

$$\kappa_1 := \inf_{1 \leq j \leq p} \inf_{\beta \neq \mathbf{0}, \beta \in A_j} \frac{\beta^\top \sum_{i=1}^n \Phi(\mathbf{X}_{i,-j}) \Phi(\mathbf{X}_{i,-j})^\top \beta}{n \|\beta\|_2^2} > \kappa > 0.$$

Assumption 3 is a restricted eigenvalue condition [8], which holds with high probability when $\Phi(\mathbf{X})$ follows a sub-Gaussian [33] or sub-exponential distribution [1].

The following lemma shows the theoretical property of the $\hat{\beta}_j$.

Lemma 1. Under Assumptions 2–3, for any constant $C > 0$, there exist positive constants $C_1, C_2, C_3 > 0$, with the choice $\lambda_1 = C_1 \sqrt{\log\{\max(n, p)\}/n}$, the following bounds hold with

probability at least $1 - \exp[-C \log\{\max(n, p)\}]$ for all $1 \leq j \leq p$:

$$\|\widehat{\boldsymbol{\beta}}_j - \boldsymbol{\beta}_j\|_2 \leq C_2 \sqrt{s_1 \log\{\max(n, p)\}/n} \text{ and } \|\widehat{\boldsymbol{\beta}}_j - \boldsymbol{\beta}_j\|_1 \leq C_3 s_1 \sqrt{\log\{\max(n, p)\}/n}. \quad (7)$$

Following Lemma 1, we establish the theoretical properties of the second-stage quantile regression. Rather than analyzing the global minimizer of the nonconvex objective, we focus on the theoretical behavior of the estimator obtained via the LLA. Let $(\widehat{\boldsymbol{\gamma}}_{j,k}^{(0)}, \widehat{b}_{j,k}^{(0)})_{k=1}^K$ denote the solution to the penalized composite quantile regression problem

$$\{(\widehat{\boldsymbol{\gamma}}_{j,k}^{(0)}, \widehat{b}_{j,k}^{(0)})\}_{k=1}^K = \underset{\{(\boldsymbol{\gamma}_k, b_k)\}_{k=1}^K}{\operatorname{argmin}} \sum_{k=1}^K \left[\frac{1}{n} \sum_{i=1}^n \rho_{\tau_k} \{ \widehat{Y}_{i,j} - \boldsymbol{\Psi}(\mathbf{X}_{i,-j})^\top \boldsymbol{\gamma}_k - b_k \} + \lambda_2 \|\boldsymbol{\gamma}_k\|_1 \right],$$

where $\widehat{Y}_{i,j} = \log |X_{i,j} - \boldsymbol{\Phi}(\mathbf{X}_{i,-j})^\top \widehat{\boldsymbol{\beta}}_j|$. Then, the LLA estimator is defined as

$$\begin{aligned} (\widehat{\boldsymbol{\gamma}}_{j,k}, \widehat{b}_{j,k})_{k=1}^K &= \underset{(\boldsymbol{\gamma}_k, b_k)_{k=1}^K}{\operatorname{argmin}} \sum_{k=1}^K \left[\frac{1}{n} \sum_{i=1}^n \rho_{\tau_k} \{ \widehat{Y}_{i,j} - \boldsymbol{\Psi}(\mathbf{X}_{i,-j})^\top \boldsymbol{\gamma}_k - b_k \} + \lambda_2 \|\boldsymbol{\gamma}_{j,k}\|_1 \right] \\ &\quad + \sum_{k=1}^K P'_{\lambda_3} (\|\widehat{\boldsymbol{\gamma}}_{j,k}^{(0)} - \widehat{\boldsymbol{\gamma}}_{j,k+1}^{(0)}\|_2) \|\boldsymbol{\gamma}_{j,k} - \boldsymbol{\gamma}_{j,k+1}\|_2. \end{aligned}$$

To facilitate the theoretical analysis, we also impose regularity conditions on the covariate $\boldsymbol{\Psi}(\mathbf{X}_{-j})$ and the regression error $\log |\varepsilon'_j|$ for $j = 1, \dots, p$.

Assumption 4. The K is bounded above by a fixed constant and the pre-selected quantiles satisfy $\tau_0 \leq \min_{1 \leq k \leq K} \{\tau_k\} \leq \max_{1 \leq k \leq K} \{\tau_k\} \leq 1 - \tau_0$ for a fixed constant $0 < \tau_0 < 1$. The τ_k th quantile of $\log(|\varepsilon'_j|)$ satisfies $Q_{\tau_k}(X_j \mid \mathbf{X}_{-j}) = \boldsymbol{\Psi}(\mathbf{X}_{-j})^\top \boldsymbol{\gamma}_{j,k} + r_{j,k}^{(g)} + b_{j,k}$ where $\|\boldsymbol{\gamma}_{j,k}\|_0 \leq s_2$ and the approximation error satisfies $\|r_{j,k}^{(g)}\|_2^2 \leq C s_2/n$ for a constant $C > 0$ and $1 \leq j \leq p$ and $1 \leq k \leq K$. The k th component of $\boldsymbol{\Psi}(\mathbf{X}_{-j})$ satisfying Cramér's condition for $1 \leq j \leq p$, $1 \leq k \leq c_d \cdot p$.

Assumption 4, analogous to Assumption 2, requires that the regression coefficients are sparse and that the approximation errors remain small. Moreover, when X_j is a sink node, the transformed error term admits the representation $\boldsymbol{\Psi}(\mathbf{X}_{i, \text{PA}^G(j)})^\top \boldsymbol{\gamma}_j^* + r_{i,j}^{(g)} + \log |\varepsilon_j|$. Under this setting, the conditional quantile regression parameters satisfy $\boldsymbol{\gamma}_{j,1} = \dots = \boldsymbol{\gamma}_{j,K}$ and the non-zero elements of $\boldsymbol{\gamma}_{j,1}$ are identical to $\boldsymbol{\gamma}_j^*$.

Assumption 5. Let the residual in the conditional quantile regression model be defined as $u_j := \log |\varepsilon'_j| - \Psi(\mathbf{X}_{-j})^\top \boldsymbol{\gamma}_{j,k} - b_{j,k} - r_{j,k}^{(g)}$. The conditional distribution of u_j given \mathbf{X}_{-j} admits an absolutely continuous density $f_{u_j|\mathbf{X}_{-j}}(\cdot)$, such that $\inf_{1 \leq j \leq p} \inf_{1 \leq k \leq K} f_{u_j|\mathbf{X}_{-j}}(0) \geq \underline{f}$ and $\sup_{1 \leq j \leq p} \sup_{1 \leq k \leq K} \sup_{t \in \mathbb{R}} \{f_{u_j|\mathbf{X}_{-j}}(t), \frac{\partial}{\partial t} f_{u_j|\mathbf{X}_{-j}}(t)\} \leq \bar{f}$, and the density function $f_{u_j|\mathbf{X}_{-j}}(\cdot)$ has sub-exponential tail.

Assumptions 4–5 collectively impose standard regularity conditions for the composite quantile regression. We assume that K is finite, since identification of sink nodes can be achieved by comparing over a finite collection of quantile levels. The boundedness of the quantile levels τ_1, \dots, τ_K is a common assumption and is essential for controlling the quantile variance. The smoothness condition is standard in the quantile regression literature [72, 3, 20, 53]. The tail assumption covers many commonly encountered distributions and is pivotal for our analysis due to the log transformation.

Assumption 6. For $\forall j \in [p]$, $k \in \{1, \dots, K\}$ and some constant $c_0 \geq 1$, define $A_j = \{\boldsymbol{\gamma} \mid \|\boldsymbol{\gamma}_{T_{j,k}^c}\|_1 \leq c_0 \|\boldsymbol{\gamma}_{T_{j,k}}\|_1\}$, where $T_{j,k}$ is the support set of $\boldsymbol{\gamma}_{j,k}$. Then

$$\kappa_2 := \inf_{1 \leq j \leq p} \inf_{1 \leq k \leq K} \inf_{\boldsymbol{\gamma} \neq \mathbf{0}, \boldsymbol{\gamma} \in A_j} \frac{\boldsymbol{\gamma}^\top \sum_{i=1}^n \boldsymbol{\Psi}(\mathbf{X}_{i,-j}) \boldsymbol{\Psi}(\mathbf{X}_{i,-j})^\top \boldsymbol{\gamma}}{n \|\boldsymbol{\gamma}\|_2^2} \geq \kappa > 0,$$

and

$$q := \inf_{1 \leq j \leq p} \inf_{1 \leq k \leq K} \inf_{\boldsymbol{\gamma} \neq \mathbf{0}, \boldsymbol{\gamma} \in A_j} \frac{\mathbb{E}[\|\boldsymbol{\Psi}(\mathbf{X}_{-j})^\top \boldsymbol{\gamma}\|^2]^{3/2}}{\mathbb{E}[\|\boldsymbol{\Psi}(\mathbf{X}_{-j})^\top \boldsymbol{\gamma}\|^3]} > 0.$$

The RNI condition [3] governs the accuracy of the quadratic approximation to the quantile regression loss over a restricted parameter set.

We now establish the convergence rate of the proposed second-stage quantile regression estimator.

Theorem 3. *Under the conditions in Lemma 1 and Assumptions 4–6, for any constant $C > 0$, the following events hold with probability at least $1 - \exp[-C \log\{\max(n, p)\}]$: for all $j \in [p]$ and $k \in [K]$, there exist constants $C_1, C_2, C_3 > 0$ such that, with the choices $\lambda_2 = C_2 \sqrt{s_1 \log\{\max(n, p)\}/n}$ and $\lambda_3 = C_3 \sqrt{s_1 s_2 \log\{\max(n, p)\}/n}$, we have*

$$\|\boldsymbol{\gamma}_{j,k} - \widehat{\boldsymbol{\gamma}}_{j,k}\|_2 \leq C_1 \sqrt{\frac{s_1 s_2 \log\{\max(n, p)\}}{n}} \quad \|\boldsymbol{\gamma}_k - \widehat{\boldsymbol{\gamma}}_k\|_1 \leq C_1 s_2 \sqrt{\frac{s_1 \log\{\max(n, p)\}}{n}}. \quad (8)$$

Moreover, the following structural recovery results hold:

1. if $\Delta_{max} = \max_{1 \leq k \leq K-1} \|\gamma_{j,k} - \gamma_{j,k+1}\|_2 \geq C_4 \sqrt{s_2} \lambda_2$ for a constant $C_4 > 0$, then

$$\hat{\gamma}_{j,k} \neq \hat{\gamma}_{j,k+1} \quad \text{for all } k \in [K] \text{ such that } \|\gamma_{j,k} - \gamma_{j,k+1}\|_2 = \Delta_{max}.$$

2. if $\gamma_{j,1} = \dots = \gamma_{j,K}$, then $\hat{\gamma}_{j,1} = \dots = \hat{\gamma}_{j,K}$.

Theorem 3 establishes two key results: convergence of the proposed second-stage estimator and consistent recovery of the structure of the quantile regression parameters. Different from the first-stage regression, the error bound in the second stage is inflated by a factor of $\sqrt{s_1}$. This is due to the second-stage response depends on estimated residuals in the first stage. Similar phenomena have been observed in two-stage estimation [71, 41]. When X_j is a sink node, Theorem 3 implies that X_j is correctly identified as a sink node according to the criterion in Section 3. When X_j is not a sink node and *signal strength* satisfies $\Delta_{max} \geq C_4 \sqrt{s_2} \lambda_2$, Theorem 3 guarantees that the corresponding estimates are not shrunk to a common value. Under the decision rule in Section 3, the node X_j is therefore correctly classified as a non-sink node.

4.2 Consistency for topological order and graph structure

This section establishes the theoretical properties of the estimated topological order and graph structure obtained from the proposed RESQUE procedure, as summarized in Algorithm 1. We first show the consistency of the estimated topological order.

To formalize the analysis, we introduce the notion of topological layers [16, 69] of a DAG G . For the unknown graph G , a single iteration of our procedure, which involves a total of $|G|$ regression analyses, identifies all sink nodes consistently, as established in Theorem 3. Algorithm 1 then iteratively detects sink nodes and removes them from the graph. The sink nodes identified in the first iteration constitute the first topological layer of G . After their removal, the sink nodes of the resulting subgraph form the second topological layer. This process continues until the graph is exhausted. Provided that each iteration correctly

identifies the sink nodes, the total number of iterations required equals the maximum distance of any node from a sink node, which is referred to as the depth of the topological layering. For illustration, in Figure 1, the nodes $N_1 = \{X_7, X_8, X_9\}$ are all sink nodes of G and thus form the first topological layer. After removing N_1 , the nodes $N_2 = \{X_5, X_6\}$ become sink nodes in the reduced graph, placing them in the second layer. This procedure is repeated until the final layer $N_T = \{X_1, X_2\}$. A formal definition is given below.

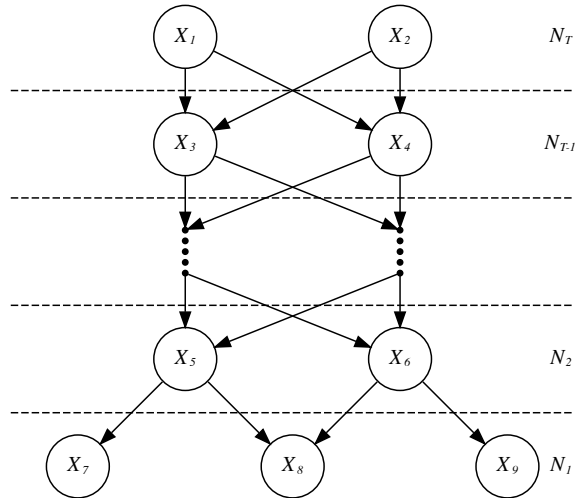


Figure 1: Illustration of the topological-layer decomposition of a DAG.

Suppose that the true DAG G admits a decomposition into T topological layers. Define $N_1 \subset [p]$ as the collection of sink nodes of G , corresponding to the first layer of G . We construct the remaining layers by iteratively partitioning the nodes as

$$N_l := \{i \in [p] / (N_1 \cup \dots \cup N_{l-1}) : X_i \text{ is a sink node of graph } G / (N_1 \cup \dots \cup N_{l-1})\},$$

where $G / (N_1 \cup \dots \cup N_{l-1})$ denotes the subgraph obtained by removing the nodes $N_1 \cup \dots \cup N_{l-1}$ and corresponding edges from G . Analogously, let \hat{N}_1 be the set of sink nodes identified in the first iteration of the RESQUE algorithm. For $l \geq 2$, define

$$\hat{N}_l := \{i \in [p] / (\hat{N}_1 \cup \dots \cup \hat{N}_{l-1}) : \text{sink nodes identified at the } l\text{th iteration of RESQUE}\},$$

where \hat{T} denotes the total number of iterations performed by the algorithm. The collection

$\{\widehat{N}_l\}_{l=1}^{\widehat{T}}$ is the estimated topological layers of the graph. For each l , let $\widehat{G}_l = G/\{\widehat{N}_1 \cup \dots \cup \widehat{N}_{l-1}\}$ denote the reduced graph and $|\widehat{G}_l|$ denote the number of nodes.

We now state the assumptions required for the theoretical analysis. Assumptions 3–6 are stated for the full graph G and specify both the notation and conditions. When we assert that these assumptions hold for a subgraph $G \subseteq G'$, this assertion is to be interpreted as the imposition of the same conditions after restricting all relevant notation and random variables to the index set corresponding to G' . Assumption 7 generalizes the conditions in Lemma 1 and Theorem 3 from a single iteration to the multi-layer setting.

Assumption 7 (Regularity conditions on the Graph). The DAG G has the topological layer decomposition $G = N_1 \cup \dots \cup N_T$, where the number of layers satisfies $T = O(n)$. For any $l \in \{1, \dots, T\}$, define $G_l = G/\{N_1 \cup \dots \cup N_{l-1}\}$ as the subgraph obtained by removing the nodes in the first $l - 1$ layers and corresponding edges. The conditions in Theorem 3 hold for every node $j \in G_l$ and $l = \{1, \dots, T\}$.

Theorem 4. *Suppose that Assumption 7 holds. For each iteration l , let the penalty parameters be chosen as $\lambda_1 = C_1 \sqrt{\log(\max(|\widehat{G}_l|, n))/n}$, $\lambda_2 = C_2 \sqrt{s_1 \log(\max(|\widehat{G}_l|, n))/n}$ and $\lambda_3 = C_2 \sqrt{s_1 s_2 \log(\max(|\widehat{G}_l|, n))/n}$, for positive constants C_1, C_2, C_3 . Then, with probability at least $1 - \exp(-C \log(n))$, the RESQUE algorithm recovers the topological ordering, in the sense that $\widehat{T} = T$ and $\widehat{N}_l = N_l$ for all $l \in [T]$.*

Theorem 4 shows that the proposed method correctly recovers the true topological order by repeatedly applying Theorem 3 to identify sink nodes at each iteration. In contrast to methods based on conditional independence testing after regression, our approach allows for approximate sparsity and thus provides greater flexibility. Once a causal order is obtained, regularized regression can be used to estimate the full graph. We show below that, under additional assumptions, the proposed method consistently recovers the true graph G .

Assumption 8 (Signal conditions). For any subgraph G_l of the true underlying graph G and any $j \in G_l$, the approximation errors satisfy $r_j^{(f)} = r_j^{(g)} = 0$ and the true parameters in 2 satisfy $\beta_{j,\min} := \max_{\beta_{j,i} \neq 0} |\beta_{j,i}| \geq a\lambda'_1$ and $\gamma_{j,\min} := \max_{\gamma_{j,i} \neq 0} |\gamma_{j,i}| \geq a\lambda'_2$

where the penalty parameters are given by $\lambda'_1 = C_1 \sqrt{s_1 \log(\max(|G_l|, n))/n}$ and $\lambda'_2 = C_2 \sqrt{s_1 s_2 \log(\max(|G_l|, n))/n}$ for some positive constants a, C_1, C_2 .

Theorem 5 (Graph recovery via penalized regression). *Suppose the conditions in Theorem 4 and Assumption 8 hold. Then, the proposed concave penalty method consistently estimates the graph G in the sense that*

$$\mathbb{P}(\hat{G} = G) \rightarrow 1 \text{ as } n \rightarrow \infty.$$

Theorem 5 establishes that, under mild conditions on the strength of the mean and variance coefficients, the proposed method recovers the true graph G with probability approaching one. Estimation of the DAG G relies on selection consistency, which is guaranteed by the strong oracle optimality [14]. In high-dimensional linear regression, consistent identification of non-zero coefficients frequently requires additional conditions [68, 32]. Especially, [69, 42] employs the irrepresentability condition for the design matrix. However, as highlighted by [42], the irrepresentability condition applied to the undirected graph imposes constraints on the graph structure that are challenging to verify in practical scenarios. Therefore, our proposed method is applicable to a broader range of DAGs than the method introduced by [69].

The signal strength conditions in Assumption 8 for the mean parameters are consistent with those required for oracle estimation in high-dimensional linear regression; see [14]. The appearance of the factor $\sqrt{s_1}$ arises from converting an ℓ_2 error bound into an ℓ_∞ bound. Under the cone invertibility factor condition of [61], this factor can be removed by strengthening the ℓ_∞ error bound. Likewise, compared with the standard oracle conditions, Assumption 8 imposes a stronger signal condition for the variance parameters. The additional factor $\sqrt{s_1}$ is required because the second-stage regression is based on the first-stage fit, as detailed in Theorem 3.

Although penalized regression methods can accurately recover the true support sets, the LLA procedure entails additional computational cost, as it requires solving both ℓ_1 penalized linear regressions and ℓ_1 penalized quantile regressions. In fact, estimation of

the graph structure G only requires identifying the supports of β_j and γ_j , which can be accomplished by selecting coefficients of sufficiently large magnitude. We consider a computationally simpler alternative to the LLA procedure based on *hard thresholding* of the initial estimators $\hat{\beta}_j$ and $\hat{\gamma}_j$. By discarding variables with small estimated coefficients, the hard-thresholding approach achieves *sign consistency* in high-dimensional linear regression under slightly stronger conditions than those required for concave penalized estimation; see [32]. The following theorem shows that, under strengthened signal strength conditions, the proposed hard-thresholding procedure reconstructs the true graph G with probability approaching one.

Theorem 6 (Graph recovery via hard-thresholding). *Suppose that the conditions of Theorem 5 hold. For any subgraph G_l and $j \in G_l$, assume that the true parameters in (2) satisfy $\beta_{j,\min} := \max_{\beta_{j,i} \neq 0} |\beta_{j,i}| \gg t_n \lambda'_1$ and $\gamma_{j,\min} := \max_{\gamma_{j,i} \neq 0} |\gamma_{j,i}| \gg t_n \lambda'_2$ for a positive sequence t_n , where λ'_1 and λ'_2 are defined as in Assumption 8. Then the proposed hard-thresholding procedure consistently recovers the true graph G in the sense that*

$$\mathbb{P}(\hat{G} = G) \rightarrow 1 \text{ as } n \rightarrow \infty.$$

5 Empirical Studies

This section evaluates the finite-sample performance of RESQUE across various settings. Section 5.1 conducts simulation studies, and Sections 5.2–5.3 examine the proposed method using two real data benchmarks.

5.1 Synthetic Experiments

In simulation studies, we investigate whether RESQUE can accurately recover the underlying causal graph and compare its performance with other popular causal discovery methods.

Competing methods. We compare with other popular causal structure learning algorithms, including causal additive models (CAM) [10], which uses high-dimensional sparse regression technique and is specifically designed for high-dimensional Gaussian noise models, rank-PC [19] uses Pearson correlation in PC algorithm [24] to improve the performance for non-Gaussian data, TL [69] which improves the RESIT algorithm [40] using sparse high-dimensional regression to detect the directed edges when determining the topological order, and non-combinatorial optimization via trace exponential and augmented lagrangian for structure learning [70, 2, NOTEARS]. We utilize the R package CAM with default parameters to implement CAM. To implement rank-PC, we first used the R package pcalg [24] to obtain a complete partially directed acyclic graph (CPDAG). Then, we employed the build-in function pdag2dag [63] in pcalg to derive a DAG. We follow the method in [69] using the graphical Lasso [15] algorithm with a fixed regularization parameter and the independence test based on distance covariance measure. The significance level of independent tests in rank-PC and TL is set to 0.01 as used by [69]. We implement NOTEARS by the Python package notears [70, 2].

Data settings. The data are generated from the following structural equation model:

$$X_j = \mathbf{X}_{\text{PA}^G(j)}^\top \boldsymbol{\beta}_j + \exp(\mathbf{X}_{\text{PA}^G(j)}^\top \boldsymbol{\gamma}_j) \varepsilon_j \quad \text{for } j = 1, \dots, p.$$

The adjacency matrix $\mathbf{U} \in \{0, 1\}^{p \times p}$ denotes the underlying DAG where $U_{j,k} = 1$ if $j \in \text{PA}^G(k)$ and $U_{j,k} = 0$ otherwise. The DAG is generated using one of three mechanisms:

- *Random graph (random).* We consider a graph where edges are added independently with equal probability. Specifically, the adjacency matrix \mathbf{U} is generated at random according to the following rule: $\Pr(U_{jk} = 1) = s$ if $j < k$, and $\Pr(U_{jk} = 1) = 0$ otherwise. Here, the parameter s controls the total number of edges present in the DAG. In the simulation, we choose $s = 1/p$ as in [27].
- *Complete tree graph (TR).* We are focused on the k -ary complete tree graph, a specialized type of tree graph, where all vertices except for certain leaves have exact k

children. To start, we create a random k -ary complete tree graph, where each vertex is a simple random sample without replacement of p nodes. The adjacency matrix is then determined based on the generated tree graph, with $U_{jl} = 1$ if node j is a child of node l . The above-generation process is a modification of the procedure discussed by [69]. In our simulation, we use $k = 2$ for the low-dimension setting and $k = 3$ for the high-dimension setting.

- *Scale-free graph (SF)*. The graph is also known as *Barabási–Albert* graph. To create a new graph, we iteratively add a new node and then select k existing vertices from the graph with the probability proportional to the number of existing edges. The selected nodes are connected to the added node. The generated graph is then processed by removing cycles to obtain a DAG. In the simulation, we choose $k = 1$ as in [70].

Notice that CAM, TL, and NOTEARS are not designed for detecting the structure via the error variance component. For a comprehensive comparison, we consider the weak heterogeneity settings for parameters $\{\beta_j, \gamma_j\}_{j=1}^p$. Each component of the mean coefficients β_j is generated independently and identically from $\text{Unif}([-1, -0.5] \cup [0.5, 1])$. Each component of the variance coefficients γ is generated independently and identically from $\text{Unif}([-1/4, -1/6] \cup [1/4, 1/6])$. In the weak heterogeneity setting, the structure information is partially available through the conditional variance. For error terms, we consider three different settings:

- *Uniform*: The random error ε_j is generated independently and identically from the uniform distribution from $[-1, 1]$.
- *Beta*: The random error ε_j is generated independently and identically from the centered Beta distribution with shape parameters $(2, 3)$.
- *Gaussian*: The random error ε_j is generated independently and identically from the Gaussian distribution with mean 0 and variance 1.

The Gaussian distribution is often used as a standard for random errors in simulating DAG. The uniform distribution is a bounded symmetric probability distribution that remains

bounded after taking the exponential. Compared to the uniform distribution, the Beta distribution has non-zero skewness.

Throughout the simulations, we set $n = 200$ and consider low-dimension settings when $p \in \{5, 10, 15, 20\}$ and high-dimension settings when $p \in \{50, 75, 100\}$.

Metrics. We evaluate the numerical performance based on four graph metrics: false discovery rate (FDR), false positive rate (FPR), true positive rate (TPR), and structural Hamming distance (SHD). To compute the metrics, let TP, RE, and FP be the numbers of identified edges with correct directions, those with wrong directions, and estimated edges not in the skeleton of the true graph. Moreover, denote by PE the total number of estimated edges, TN the number of correctly identified non-edges, and FN the number of missing edges compared to the true skeleton. Then

$$\begin{aligned} \text{FDR} &= (\text{RE} + \text{FP})/\text{PE}, & \text{FPR} &= (\text{RE} + \text{FP})/(\text{FP} + \text{TN}), \\ \text{TPR} &= \text{TP}/(\text{TP} + \text{FN}), & \text{SHD} &= \text{FP} + \text{FN} + \text{RE}. \end{aligned}$$

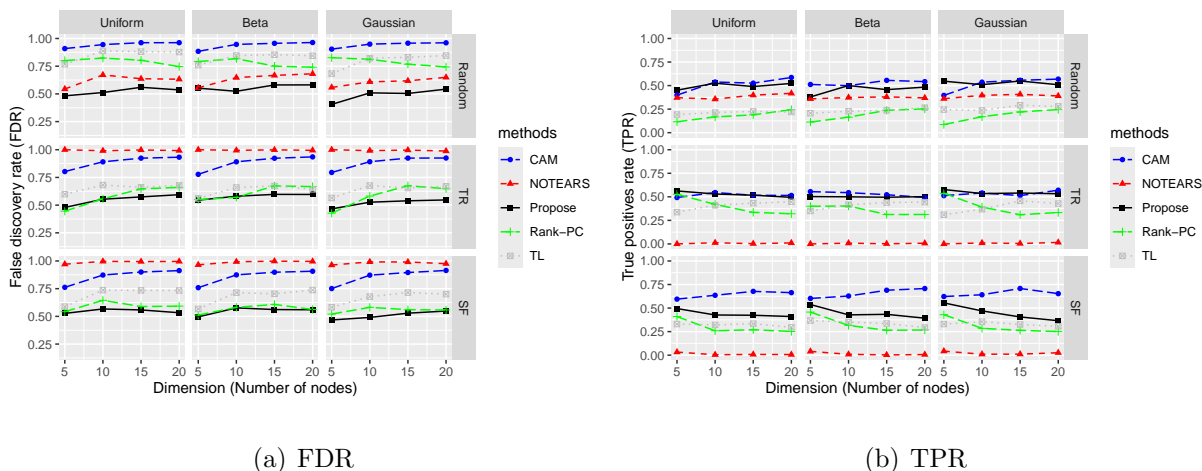


Figure 2: Empirical performance of CAM, rank-PC, TL, NOTEARS, and the proposed method in low-dimensional settings. False discovery rates and true positive rates in various graph structures and error distributions are presented.

Results. The results for low- and high-dimensional settings are shown in Figures 2–3, respectively. In all settings, RESQUE has high true discovery rates with relatively low false

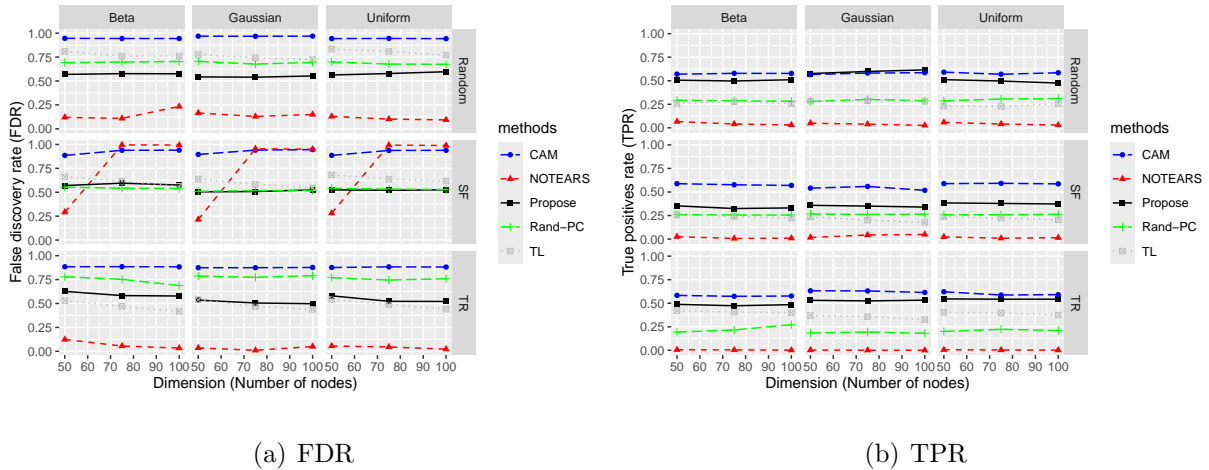


Figure 3: Empirical performance of CAM, rank-PC, TL, NOTEARS, and RESQUE in high-dimensional settings. False discovery rates and true positive rates in various graph structures and error distributions are presented.

discovery rates. For example, in low-dimensional settings, it has the lowest FDR among all methods. It has nearly the highest TPR among all methods when the underlying graph is generated from Random and TR. When the underlying graph is SF, the proposed method still has a TPR higher than all other methods except CAM. Notice that CAM has a very high FDR and thus results in very high SHD, as shown in the appendix. Thus, the proposed method outperforms all other methods in the low-dimension settings. Similar results are shown in the high-dimensional settings; other than that, the NOTEARS has a very low FDR. Note that the performance of NOTEARS is sensitive to the scale of variables. After standardizing the variables, the NOTEARS shows nearly zero TPR in the high-dimensional settings. Thus, the proposed method outperforms all other methods in the high-dimension settings. We make some further comments about the SF graph. The critical requirement of our proposed method is the sparsity assumption; that is, the number of parents of every node is relatively small. A scale-free network has the property that the number of edges originating from a given node exhibits a power law distribution. Power law degree distributions alone imply that some nodes in the tail of the power law must have a high degree, which implies violating the sparsity assumption for some nodes. However, RESQUE

still has reasonable performance.

5.2 Sachs’ flow cytometry dataset

Dataset. In this section, we consider the flow cytometry dataset [43], which includes continuous concentrations of the molecules of numerous phosphorylated proteins and phospholipid components found in thousands of individual primary human immune system cells. The initial analysis sought to understand the causal pathways connecting a group of $p = 11$ proteins using $n = 7466$ observations from observational and experimental data under a series of stimulatory cues and inhibitory interventions. For evaluation, we use the *consensus graph*, which is created by combining results from various experimental annotations, and is widely accepted as a reference causal graph by the biological community. The dataset comprises observations from nine distinct environments. As indicated in [45], observations from all but one environment do not follow *homoscedastic linear structural equations*.

Results. In Table 1, we compare RESQUE with other methods via the number of correct estimated edges and the total structural Hamming distance. RESQUE successfully identifies 13 out of 20 directed edges in the consensus graph with the highest true positive rate among all methods and the smallest SHD. We make some further discussions of other competing methods. Coinciding with the observations in Section 5.1, CAM has a relatively high TPR, detecting 12 out of 20 edges in the consensus but suffers from high false positives. The performance of Rank-PC is relatively weak compared to other recent methods, and TL and NOTEARS are based on linear structural equations and only identify edges through the conditional expectation, and thus have similar performances.

| | CAM | NOTEARS | Rank-PC | TL | RESQUE |
|-----------------|-----|---------|---------|----|--------|
| # Correct Edges | 12 | 7 | 6 | 6 | 13 |
| SHD | 51 | 22 | 35 | 21 | 14 |

Table 1: Comparison results of the Sachs dataset.

Figure 4 displays a detailed comparison of the estimated causal graph by RESQUE and the consensus graph. It shows that 4 out of 13 correctly identified edges are only identified through the variance component. In comparison, 2 out of 13 correctly identified edges are only identified through the mean component. The result suggests that the observations in the Sachs’ dataset have a nontrivial heteroscedasticity, agreeing with [45]. RESQUE identifies 9 out of 20 edges through the mean component. Note that the actual causal relations for Sachs’ data have yet to be discovered. Some directed edges identified by our proposed method, while not included in the consensus graph, have also been reported by other methods: For instance, the directed edges from PKC to PKA and PKC to PKA are reported by [34]. Overall, RESQUE performs well on the Sachs dataset.

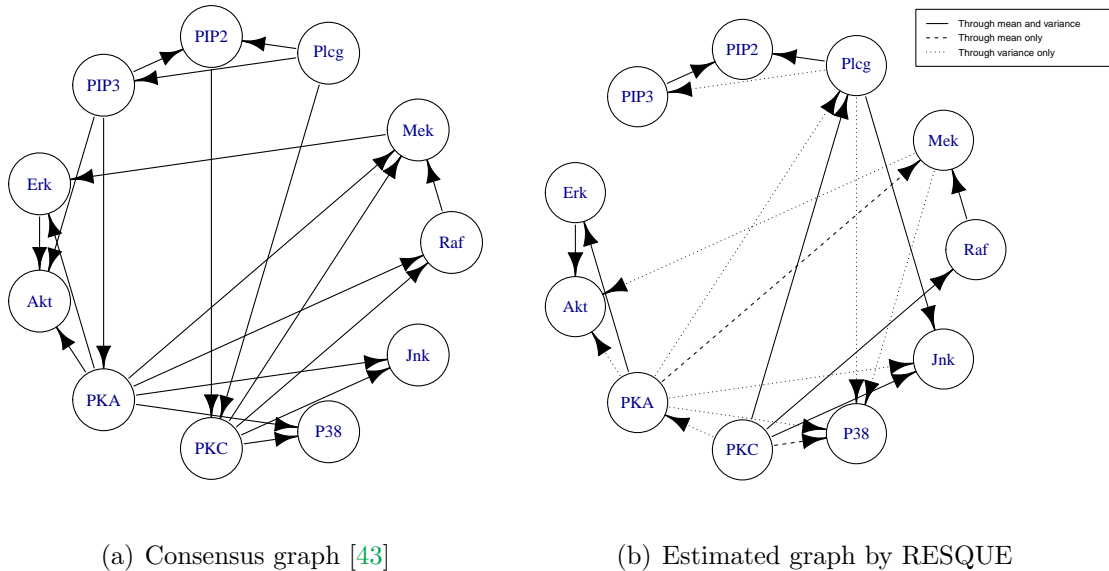


Figure 4: Consensus graph and estimated graph by RESQUE using the Sachs dataset.

5.3 CauseEffectPairs collection

Dataset. This section considers the CauseEffectPairs collection [35], which consists of 108 datasets, each containing samples of a pair of random variables, where one variable is known to cause the other. The goal is to determine, for each pair, which variable is the cause and which is the effect, based solely on the observed samples. Each dataset in the CauseEffectPairs collection meets the following criteria: it contains at least a few hundred

samples per pair, a significant causal relation exists between the two variables, and the direction of the causal relation is known. Some pairs contain high-dimensional variables. We thus selected 99 pairs out of 108 for further analysis, where each variable in the pair is univariate. See [35] for further details.

| | CAM | Rank-PC | NOTEARS | TL | RESQUE |
|----------|-------|---------|---------|-------|--------|
| Accuracy | 0.567 | 0.258 | 0.258 | 0.361 | 0.711 |

Table 2: Accuracy of CAM, NOTEARS, DAGMA, Rank-PC, and the proposed method evaluated on CauseEffectPairs collection.

Results. We evaluate the performance by comparing the accuracy of causal discovery, defined as the proportion of the corrected estimated causal directions. As shown in Table 2, RESQUE performs well compared to other competing methods. We also note that CAM has relatively good performance, and the weak performances of TL and NOTEARS are partly due to the violations of their model assumptions: As shown by [35], the scatter plots of many pairs exhibits nonlinearity and heteroscedasticity.

6 Discussion

This paper studies causal discovery under additive heteroscedastic structural equation models. We have established comprehensive identifiability results for a location-scale noise causal model and propose RESQUE, a two-stage regression strategy to recover the topological order and estimate the underlying DAG. Our results highlight that heteroscedasticity encodes causal direction beyond what is identifiable from the conditional mean alone, and can be systematically leveraged for causal structure learning.

We discuss several directions that are worth pursuing. First, [65] fully characterized non-identifiable cases of post-nonlinear causal models. It remains open and would be interesting to investigate whether similar results can also be obtained for heteroscedastic SEMs. Second, the proposed method assumes causal sufficiency, whereas many applications

involve latent confounding and correlated errors [27]; extending the proposed framework to such settings would be a natural direction. Finally, inference after causal discovery remains challenging [26]: constructing valid confidence sets for discovered edges/orders [57], or for causal effects derived from an estimated graph [18, 11], requires careful accounting for the selection inherent in the discovery process.

Acknowledgment

This research did not receive any specific grant from funding agencies in public, commercial, or not-for-profit sectors. The work was carried out as part of the authors’ routine academic duties at their respective institutions, in the absence of any commercial, financial, or institutional relationships that could be construed as a potential conflict of interest.

References

- [1] R. Adamczak, A. E. Litvak, A. Pajor, and N. Tomczak-Jaegermann. Restricted isometry property of matrices with independent columns and neighborly polytopes by random sampling. *Constructive Approximation*, 34:61–88, 2011.
- [2] K. Bello, B. Aragam, and P. Ravikumar. DAGMA: Learning DAGs via M-matrices and a Log-Determinant Acyclicity Characterization. In *Advances in Neural Information Processing Systems*, 2022.
- [3] A. Belloni and V. Chernozhukov. l1-penalized quantile regression in high-dimensional sparse models. *The Annals of Statistics*, 39(1):82 – 130, 2011.
- [4] A. Belloni, V. Chernozhukov, and C. Hansen. Inference for high-dimensional sparse econometric models. *arXiv preprint arXiv:1201.0220*, 2011.
- [5] A. Belloni, V. Chernozhukov, and K. Kato. Valid post-selection inference in high-dimensional approximately sparse quantile regression models. *Journal of the American Statistical Association*, 114(526):749–758, 2019.
- [6] P. M. Bentler. Causal modeling via structural equation systems. In *Handbook of multivariate experimental psychology*, pages 317–335. Springer, 1988.
- [7] J. Berrevoets, J. Raymaekers, M. Van der Schaar, T. Verdonck, and R. Yao. Differentiable causal structure learning with identifiability by notime. In *Proceedings of machine learning research*, volume 258, pages 3115–3123. PMLR, 2025.

- [8] P. J. Bickel, Y. Ritov, and A. B. Tsybakov. Simultaneous analysis of lasso and dantzig selector. *The Annals of Statistics*, 37(4):1705–1732, 2009.
- [9] P. Blöbaum, D. Janzing, T. Washio, S. Shimizu, and B. Schölkopf. Cause-effect inference by comparing regression errors. In *International Conference on Artificial Intelligence and Statistics*, pages 900–909. PMLR, 2018.
- [10] P. Bühlmann, J. Peters, and J. Ernest. CAM: Causal additive models, high-dimensional order search and penalized regression. *The Annals of Statistics*, 42(6):2526 – 2556, 2014.
- [11] T.-H. Chang, Z. Guo, and D. Malinsky. Post-selection inference for causal effects after causal discovery. *Biometrika*, 113(1):asaf073, 2026.
- [12] D. M. Chickering. Optimal structure identification with greedy search. *Journal of machine learning research*, 3(Nov):507–554, 2002.
- [13] J. Fan and R. Li. Variable selection via nonconcave penalized likelihood and its oracle properties. *Journal of the American statistical Association*, 96(456):1348–1360, 2001.
- [14] J. Fan, L. Xue, and H. Zou. Strong oracle optimality of folded concave penalized estimation. *Annals of statistics*, 42(3):819, 2014.
- [15] J. Friedman, T. Hastie, and R. Tibshirani. Sparse inverse covariance estimation with the graphical lasso. *Biostatistics*, 9(3):432–441, 2008.
- [16] M. Gao, Y. Ding, and B. Aragam. A polynomial-time algorithm for learning nonparametric causal graphs. *Advances in Neural Information Processing Systems*, 33:11599–11611, 2020.
- [17] C. Glymour, K. Zhang, and P. Spirtes. Review of causal discovery methods based on graphical models. *Frontiers in genetics*, 10:524, 2019.
- [18] P. Gradu, T. Zrnic, Y. Wang, and M. I. Jordan. Valid inference after causal discovery. *Journal of the American Statistical Association*, 120(550):1127–1138, 2025.
- [19] N. Harris and M. Drton. PC algorithm for nonparanormal graphical models. *Journal of Machine Learning Research*, 14(11), 2013.
- [20] X. He, X. Pan, K. M. Tan, and W.-X. Zhou. Smoothed quantile regression with large-scale inference. *Journal of Econometrics*, 2021.
- [21] C. Heinze-Deml, M. H. Maathuis, and N. Meinshausen. Causal structure learning. *Annual Review of Statistics and Its Application*, 5:371–391, 2018.
- [22] P. Hoyer, D. Janzing, J. Mooij, J. Peters, and B. Schölkopf. Nonlinear causal discovery with additive noise models. In *Twenty-Second Annual Conference on Neural Information Processing Systems (NIPS 2008)*, pages 689–696. Curran, 2009.
- [23] A. Immer, C. Schultheiss, J. E. Vogt, B. Schölkopf, P. Bühlmann, and A. Marx. On the identifiability and estimation of causal location-scale noise models. In *International Conference on Machine Learning*, pages 14316–14332. PMLR, 2023.

- [24] M. Kalisch and P. Bühlman. Estimating high-dimensional directed acyclic graphs with the pc-algorithm. *Journal of Machine Learning Research*, 8(3), 2007.
- [25] R. Koenker and G. Bassett, Jr. Regression quantiles. *Econometrica: journal of the Econometric Society*, pages 33–50, 1978.
- [26] C. Li, X. Shen, and W. Pan. Likelihood ratio tests for a large directed acyclic graph. *Journal of the American Statistical Association*, 2020.
- [27] C. Li, X. Shen, and W. Pan. Nonlinear causal discovery with confounders. *Journal of the American Statistical Association*, pages 1–10, 2023.
- [28] Y. Li, A. Torralba, A. Anandkumar, D. Fox, and A. Garg. Causal discovery in physical systems from videos. *Advances in Neural Information Processing Systems*, 33:9180–9192, 2020.
- [29] Y. Li and J. Zhu. L 1-norm quantile regression. *Journal of Computational and Graphical Statistics*, 17(1):163–185, 2008.
- [30] Y. Lin, Y. Huang, W. Liu, H. Deng, I. Ng, K. Zhang, M. Gong, Y. Ma, and B. Huang. A skewness-based criterion for addressing heteroscedastic noise in causal discovery. In *International Conference on Learning Representations*, volume 2025, pages 89283–89310, 2025.
- [31] M. H. Maathuis, D. Colombo, M. Kalisch, and P. Bühlmann. Predicting causal effects in large-scale systems from observational data. *Nature methods*, 7(4):247–248, 2010.
- [32] N. Meinshausen and B. Yu. Lasso-type recovery of sparse representations for high-dimensional data. *The Annals of Statistics*, 37(1):246–270, 2009.
- [33] S. Mendelson, A. Pajor, and N. Tomczak-Jaegermann. Uniform uncertainty principle for bernoulli and subgaussian ensembles. *Constructive Approximation*, 28:277–289, 2008.
- [34] J. M. Mooij and T. Heskes. Cyclic causal discovery from continuous equilibrium data. In *Proceedings of the Twenty-Ninth Conference on Uncertainty in Artificial Intelligence*, pages 431–439, 2013.
- [35] J. M. Mooij, J. Peters, D. Janzing, J. Zscheischler, and B. Schölkopf. Distinguishing cause from effect using observational data: methods and benchmarks. *Journal of Machine Learning Research*, 17(32):1–102, 2016.
- [36] G. Park. Identifiability of additive noise models using conditional variances. *Journal of Machine Learning Research*, 21(75):1–34, 2020.
- [37] J. Pearl. *Causality*. Cambridge university press, 2009.
- [38] J. Peters and P. Bühlmann. Identifiability of gaussian structural equation models with equal error variances. *Biometrika*, 101(1):219–228, 2014.

- [39] J. Peters, D. Janzing, and B. Schölkopf. Identifying cause and effect on discrete data using additive noise models. In *Proceedings of the thirteenth international conference on artificial intelligence and statistics*, pages 597–604. JMLR Workshop and Conference Proceedings, 2010.
- [40] J. Peters, J. M. Mooij, D. Janzing, and B. Schölkopf. Causal discovery with continuous additive noise models. *Journal of Machine Learning Research*, 15:2009–2053, 2014.
- [41] Y. Qiu, J. Tao, and X.-H. Zhou. Inference of heterogeneous treatment effects using observational data with high-dimensional covariates. *Journal of the Royal Statistical Society Series B: Statistical Methodology*, 83(5):1016–1043, 2021.
- [42] G. Raskutti, M. J. Wainwright, and B. Yu. Restricted eigenvalue properties for correlated gaussian designs. *The Journal of Machine Learning Research*, 11:2241–2259, 2010.
- [43] K. Sachs, O. Perez, D. Pe’er, D. A. Lauffenburger, and G. P. Nolan. Causal protein-signaling networks derived from multiparameter single-cell data. *Science*, 308(5721):523–529, 2005.
- [44] B. Schölkopf, F. Locatello, S. Bauer, N. R. Ke, N. Kalchbrenner, A. Goyal, and Y. Bengio. Toward causal representation learning. *Proceedings of the IEEE*, 109(5):612–634, 2021.
- [45] C. Schultheiss and P. Bühlmann. Ancestor regression in linear structural equation models. *Biometrika*, 110(4):1117–1124, 2023.
- [46] C. Schultheiss and P. Bühlmann. On the pitfalls of gaussian likelihood scoring for causal discovery. *Journal of Causal Inference*, 11(1):20220068, 2023.
- [47] S. Shimizu, P. O. Hoyer, A. Hyvärinen, A. Kerminen, and M. Jordan. A linear non-Gaussian acyclic model for causal discovery. *Journal of Machine Learning Research*, 7(10), 2006.
- [48] P. Spirtes. An anytime algorithm for causal inference. In *International Workshop on Artificial Intelligence and Statistics*, pages 278–285. PMLR, 2001.
- [49] P. Spirtes and C. Glymour. An algorithm for fast recovery of sparse causal graphs. *Social science computer review*, 9(1):62–72, 1991.
- [50] P. Spirtes, C. N. Glymour, and R. Scheines. *Causation, prediction, and search*. MIT press, 2000.
- [51] E. V. Strobl and T. A. Lasko. Identifying patient-specific root causes with the heteroscedastic noise model. *Journal of Computational Science*, 72:102099, 2023.
- [52] X. Sun and O. Schulte. Cause-effect inference in location-scale noise models: Maximum likelihood vs. independence testing. *Advances in Neural Information Processing Systems*, 36:5447–5483, 2023.

- [53] K. M. Tan, L. Wang, and W.-X. Zhou. High-dimensional quantile regression: Convolution smoothing and concave regularization. *Journal of the Royal Statistical Society Series B: Statistical Methodology*, 84(1):205–233, 2022.
- [54] Q.-D. Tran, B. Duong, P. Nguyen, and T. Nguyen. Robust estimation of causal heteroscedastic noise models. In *Proceedings of the 2024 SIAM International Conference on Data Mining (SDM)*, pages 788–796. SIAM, 2024.
- [55] I. Tsamardinos, L. E. Brown, and C. F. Aliferis. The max-min hill-climbing bayesian network structure learning algorithm. *Machine learning*, 65(1):31–78, 2006.
- [56] M. J. Vowels, N. C. Camgoz, and R. Bowden. D’ya like DAGs? a survey on structure learning and causal discovery. *ACM Computing Surveys*, 55(4):1–36, 2022.
- [57] Y. S. Wang, M. Kolar, and M. Drton. Confidence sets for causal orderings. *Journal of the American Statistical Association*, pages 1–14, 2025.
- [58] H. Wold. Causality and econometrics. *Econometrica: Journal of the Econometric Society*, pages 162–177, 1954.
- [59] S. Xu, O. A. Mian, A. Marx, and J. Vreeken. Inferring cause and effect in the presence of heteroscedastic noise. In *International Conference on Machine Learning*, pages 24615–24630. PMLR, 2022.
- [60] Y. Yang, S. Bom, and X. Shen. A hierarchical ensemble causal structure learning approach for wafer manufacturing. *Journal of Intelligent Manufacturing*, 35(6):2961–2978, 2024.
- [61] F. Ye and C.-H. Zhang. Rate minimaxity of the lasso and dantzig selector for the lq loss in lr balls. *The Journal of Machine Learning Research*, 11:3519–3540, 2010.
- [62] N. Yin, T. Gao, Y. Yu, and Q. Ji. Effective causal discovery under identifiable heteroscedastic noise model. In *Proceedings of the AAAI Conference on Artificial Intelligence*, volume 38, pages 16486–16494, 2024.
- [63] Y. Yuan, X. Shen, W. Pan, and Z. Wang. Constrained likelihood for reconstructing a directed acyclic gaussian graph. *Biometrika*, 106(1):109–125, 2019.
- [64] C.-H. Zhang. Nearly unbiased variable selection under minimax concave penalty. *Annals of statistics*, 38(2):894–942, 2010.
- [65] K. Zhang and A. Hyvärinen. On the identifiability of the post-nonlinear causal model. In *Proceedings of the Twenty-Fifth Conference on Uncertainty in Artificial Intelligence*, pages 647–655, 2009.
- [66] K. Zhang and A. Hyvärinen. Distinguishing causes from effects using nonlinear acyclic causal models. In *Causality: Objectives and Assessment*, pages 157–164. PMLR, 2010.
- [67] T. Zhang, Y. Zhang, and T. Zhou. Statistical insights into HSIC in high dimensions. *Advances in Neural Information Processing Systems*, 36:19145–19156, 2023.

- [68] P. Zhao and B. Yu. On model selection consistency of lasso. *The Journal of Machine Learning Research*, 7:2541–2563, 2006.
- [69] R. Zhao, X. He, and J. Wang. Learning linear non-gaussian directed acyclic graph with diverging number of nodes. *The Journal of Machine Learning Research*, 23(1):12314–12347, 2022.
- [70] X. Zheng, B. Aragam, P. K. Ravikumar, and E. P. Xing. Dags with no tears: Continuous optimization for structure learning. *Advances in neural information processing systems*, 31, 2018.
- [71] L. Zhou and H. Zou. Cross-fitted residual regression for high-dimensional heteroscedasticity pursuit. *Journal of the American Statistical Association*, 118(542):1056–1065, 2023.
- [72] H. Zou and M. Yuan. Composite quantile regression and the oracle model selection theory. *Annals of Statistics*, 36(3):1108–1126, 2008.